THE AMERICAN MINERALOGIST, VOL. 56, MAY-JUNE, 1971

CATION DISTRIBUTION AND ATOMIC THERMAL VIBRATIONS IN AN IRON-RICH ORTHOPYROXENE

CHARLES W. BURNHAM AND YOSHIKAZU OHASHI, *Department of Geological Sciences,*[1] *Harvard University, Cambridge, Mass. 02138*

AND

STEFAN S. HAFNER AND DAVID VIRGO,[2] *Department of the Geophysical Sciences, The University of Chicago, Chicago, Illinois 60637*

ABSTRACT

The cation distribution over the two non-equivalent sites $M1$ and $M2$ in an iron-rich orthopyroxene, $Ca_{0.04}Mg_{0.26}Fe_{1.70}Si_2O_6$, has been determined by least-squares refinement of X-ray diffraction data and from gamma-ray resonant absorption spectra. The site occupancies are $0.25Mg^{2+}+0.75Fe^{2+}$ for $M1$ and $0.04Ca^{2+}+0.96Fe^{2+}$ for $M2$. Almost all the Mg ions occur in the $M1$ site. Comparison of X-ray diffraction and resonant absorption data suggests that static non-spherical electronic effects due to partially covalent bonding contribute, perhaps significantly, to the atomic thermal ellipsoids of vibration apparent to the X-ray experiment for cations at the $M2$ sites, and possibly for one or more oxygen atoms.

INTRODUCTION

Studies over the past several years have shown that the cation distribution among the octahedrally coordinated sites in chain silicates frequently depends on the chemical composition, temperature, pressure, and cooling rate of the crystalline phase. Distribution studies are of particular interest for thermodynamic considerations. However, to obtain thermodynamic data such as cation exchange energies between different sites, equilibrium distribution constants, activation energies for ordering and disordering processes at the sites, or for the interpretation of calorimetric data, the site occupancy should be known with considerable accuracy.

Orthopyroxenes are particularly suitable chain silicates for precise site-occupancy determinations. Their crystal structure provides only two non-equivalent octahedrally-coordinated positions, $M1$ and $M2$, and the only major cations present at these positions are magnesium and iron. In this paper an attempt has been made to determine the site occupancy of an orthopyroxene with approximate composition $Ca_{0.04}Mg_{0.26}Fe_{1.70}Si_2O_6$ by two independent techniques: X-ray diffraction, and nuclear gamma-ray resonant absorption (Mössbauer effect).

Ghose (1965) showed, using X-ray diffraction, that in an intermediate orthopyroxene, $Mg_{0.93}Fe_{1.07}Si_2O_6$, from a metamorphic rock Fe^{2+} prefers the $M2$ site. Refined structural parameters have been reported for

[1] Mineralogical Contribution No. 481, Harvard University.

[2] Present address: Geophysical Laboratory, Carnegie Institution of Washington, Washington, D.C. 20008.

synthetic orthoferrosilite, $Fe_2Si_2O_6$, by Burnham (1967), and for orthoenstatite, $Mg_2Si_2O_6$, by Morimoto and Koto (1969). No further X-ray determinations of hypersthene have been carried out. However, Fe^{2+} distributions over $M1$ and $M2$ in orthopyroxenes with variable Fe/(Fe+Mg) ratios have been determined approximately from gamma-ray resonant absorption spectra of ^{57}Fe by Evans *et. al.*, (1967) and, with somewhat different results, by Bancroft, *et. al.*, (1967). The primary purpose of this study is to establish a correlation between X-ray diffraction and resonant absorption data with respect to cation distribution numbers and vibrational properties of the atoms at the sites.

Experimental

Specimen description and analysis. The orthopyroxene selected for this study has the approximate composition $Ca_{0.02}Mg_{0.28}Fe_{1.70}Si_2O_6$, and occurs in a quartz-garnet orthopyroxene granulite from Greenland, kindly provided by Professor Hans Ramberg (specimen XYZ, *cf.* also Ramberg and DeVore, 1951).[1] Microscopic examination revealed that many crystals are apparently homogeneous, but some show very small amounts of multiple exsolution lamellae. Professor Humberto Fernández-Morán kindly examined numerous crystal fragments with his 200 kV electron microscope. No lamellae structure was observed in addition to the coarse lamellae (Fernández-Morán, *et al.*, 1970).

Microprobe X-ray emission analysis of XYZ orthopyroxene was carried out using polished thin sections of the rock. Analyses for Si, Al, Mg, Fe, and Ca were made at 15 kV and 0.5 μA with a 15 μm diameter electron beam. Average readings were obtained from 12 different grains (readings from 10 spots within each grain) for five elements. Sample XYZ-Y1 was used as a standard for Si, Mg, and Fe; sample E24 for Al; and sample R2394 for Ca (*cf.* Howie and Smith, 1966). Corrections were applied according to the factors listed by Smith (1965) and Howie and Smith (1966). The elemental distribution, especially of Al and Ca, is exceptionally homogeneous in each grain. The standard errors, within the grains as well as between the grains, are one percent for Si, Mg, and Fe, and two percent for Al and Ca. It should be noted that the chemical composition of XYZ-Y1 turned out to be slightly different from that of our XYZ specimen. In addition, the amount of Fe^{3+} (four percent of total iron) as determined by the wet chemical analysis was found to be too high. Our X-ray emission analysis and Fe^{3+} determination from Mössbauer spectra is compared with previously published analyses of XYZ in Table 1.

X-ray diffraction. Unit-cell dimensions were measured using a back-reflection precision Weissenberg camera. Data for both $CuK\alpha_1$ and $K\alpha_2$ wavelengths were refined by least-squares methods (Burnham, 1962) using 69 measurements and making allowance for systematic errors due to specimen absorption, film shrinkage, and camera eccentricity. The refined cell dimensions are:

$$a = 18.405 \pm 0.001 \text{ Å},$$
$$b = 9.0338 \pm 0.0007 \text{ Å},$$
$$c = 5.2390 \pm 0.0004 \text{ Å}.$$

The cell volume is 871.08 ± 0.14Å^3; there are eight formula units ($Z=8$) per cell. Careful examination of glide-plane extinction criteria confirms space group *Pbca* for this specimen.

Intensity measurements were made with a four-circle computer-controlled diffractometer using Nb-filtered $MoK\alpha$ radiation. All reflections in one octant of reciprocal space

[1] Samples are available from S. S. Hafner.

TABLE 1. CHEMICAL FORMULA OF ORTHOPYROXENE SPECIMEN XYZ BASED ON SIX OXYGENS

	Ca	Mg	Fe^{2+}	Fe^{3+}	Mn	Ti	$Al^{(VI)}$	Si	$Al^{(IV)}$	O
(1)	0.042	0.248	1.537	0.059	0.002	0.011	0.042	1.983	0.017	6
(2)	0.038	0.259	1.680		0.003	0.004	0.010	1.992	0.008	6
(3)	0.038	0.239	1.700		—	—	0.017	1.983	0.021	6
(4)	—	—		0.013	—	—	—	—	—	6

(1) Wet chemical analysis, analyst B. Bruum (Ramberg and DeVore, 1951).
(2) Electron microprobe analysis of XYZ-Y1 (Howie and Smith, 1966)
(3) Electron microprobe analysis (Virgo and Hafner, 1969) of our XYZ specimen; (2) was used as standard for Mg, Fe, Si.
(4) From Mössbauer spectra. The determined area ratio Fe^{3+} resonant absorption to total resonant absorption of iron is 0.08 ± 0.02 (S.E.).

within the range 0.1 to 0.8 of $\sin\theta/\lambda$ were measured using $\omega - 2\theta$ scans. The counting rate was not allowed to exceed 10K/second, the linearity limit of the counting system. Integrated intensities were corrected in the usual manner for Lorentz and polarization effects. Absorption corrections were computed using numerical integration techniques (Burnham, 1966); transmission factors varied from 0.25 to 0.52 for the roughly prismatic crystal (approximately $0.12 \times 0.24 \times 0.28$ mm.) with a linear absorption coefficient of 60.92 cm^{-1} for MoKα.

Most of the structure refinement was carried out on an IBM 7094 computer using a modified version of SFLSQ, a full-matrix least squares program written by C. T. Prewitt. All observations were weighted according to $w = 1/\sigma_F^2$, where σ_F is the estimated standard deviation of the observation based on counting statistics.[1] Observations whose integrated intensities were below the minimum observable intensity ($I_{min.} = 2\sigma_I$) were rejected from the normal equations matrix. During early refinement stages, observations for which $|\Delta F| > 20$ were also rejected. In the final stages the criterion was modified to reject observations for which $|\Delta F| > 6$. On the final cycle, 25 of 1526 observed data were rejected on this basis.

[1] The estimated standard deviation of an observation, σ_F, was computed according to

$$\sigma_F = \frac{\sigma_I}{2F \cdot Lp \cdot T}$$

with

$$\sigma_I = a\left[C + \left(\frac{T_c}{2T_b}\right)^2 (B_1 + B_2)\right]^{1/2}$$

where

F = observed structure factor,
Lp = Lorentz-polarization factor,
T = transmission factor,
a = attenuator factor (if a Nb attenuator was not imposed, a is 1, otherwise a is the absorption factor of the attenuator),
C = total counts accumulated during scan,
T_c = scan counting time in seconds,
B_1, B_2 = background counts on each side of peak,
T_b = background counting time in seconds,
$T\sigma_I$ = estimated standard deviation of integrated intensity.

Scattering factors for the ions Fe^{2+}, Mg^{2+}, Ca^{2+}, Si^{4+}, and O^{2-} were used in refinement with SFLSQ. The scattering power of each ion was evaluated using

$$= \exp \sum_{n=0}^{6} a_n(\sin \theta/\lambda)^n$$

Constants, a_n, for the cations have been tabulated by Onken and Fischer (1968); those for O^{2-} were listed by Prewitt and Burnham (1966).

Least-squares refinement was initiated using positional parameters and isotropic temperature factors of orthoferrosilite (Burnham, 1967). Mg and Fe were assumed to be equally distributed over the $M1$ and $M2$ sites; the small scattering contribution from Ca as well as anomalous dispersion effects were ignored. When the R value reached 0.05, site occupancy factors for Fe and Mg in $M1$ and $M2$ were refined. SFLSQ treats each site independently, hence the total amount of each cation is not fixed and any combination of occupancy factors is mathematically possible.

Our first attempt to refine site occupancies was unsuccessful—the indicated amount of Fe in $M2$ increased to more than 100 percent, and total iron reached 1.82 atoms, considerably more than the 1.7 determined by microprobe analysis. To eliminate known systematic errors in the model, both real and imaginary anomalous dispersion terms, taken from *International Tables for X-ray Crystallography*, vol. III, p. 215 (1962), were included in subsequent calculations. In addition, the scattering contribution from 0.04 Ca atom in the $M2$ site was included. The assumption that Ca is restricted to $M2$ is, of course, based on the known preference of Ca for the analogous $M2$ site in the diopside-hedenbergite series.

Subsequent least-squares cycles using anisotropic temperature factor models reduced the R value to 0.031. Throughout this refinement stage, the content of Ca in $M2$ was fixed at 0.04 atom and the sum of Fe and Mg was fixed at 0.96 atom. The results indicate that little or no Mg (0.003 ± 0.003 atom) occupies $M2$ (see Table 2).

No external relations were imposed between the $M1$ and $M2$ occupancies. When these were varied independently, correlations[1] of the order of -0.7 between the scale factor and $M1$ and $M2$ occupancies appeared. We believe these correlations were causing the erroneously high total Fe values, hence we held the scale factor fixed during the final cycles of least-squares. This course of action seemed appropriate because scale factor variations during the early refinement stages were less than 1 percent. In the last least-squares cycle the maximum correlations between occupancy and anisotropic temperature factors were 0.4 for both metal sites. The correlation between $M1$ and $M2$ occupancy factors was 0.5.

Because the amount of Mg occupying $M2$ appears to be so small, we felt that further refinement assuming only Fe and Ca atoms occupy $M2$ would give a valid check on Ca content. Accordingly, the occupancies were offset by 5 percent, and all parameters except the scale factor were varied through two additional cycles to yield the occupancies listed in row 2 of Table 2. These results are very similar to the previous ones (row 1, Table 2), and the Ca determination is close to the 0.038 atom of Ca obtained by microprobe analysis.

R values for different sets of site occupancy factors were calculated using 366 observations sampled uniformly from the whole data set. Figure 1 shows the variation of R with occupancy, and demonstrates the existence of a fairly well-defined convergence minimum.

When the structure refinement was nearly complete, a new least-squares program, RFINE (written by L. W. Finger), became available to us for use on the IBM 360/65 computer. Since RFINE allows external constraints on total chemistry to be imposed dur-

[1] Correlation coefficients, ρ_{ij}, are the obtained from the least-squares variance-covariance matrix according to

$$\rho_{ij} = \frac{\sigma_{ij}}{(\sigma_i^2 \sigma_j^2)^{\frac{1}{2}}}$$

TABLE 2. CATION DISTRIBUTION IN XYZ ORTHOPYROXENE[a]

Experiment	$M1$ occupancy	$M2$ occupancy[b]	$Fe(M1)/(Fe(M1)+Fe(M2))$	Total Fe	$Fe^{3+}/(Fe^{2+}+Fe^{3+})$	Total $Mg+Al^{VI}$	Total Ca
X-ray diffraction; 0.04 Ca fixed in $M2$ (SFLSQ)	0.742 Fe ± .003 0.258 Mg ± .003	0.957 Fe ± .003 0.003 Mg ± .003	0.437	1.699	—	0.261	(0.040)
X-ray diffraction; Mg omitted from $M2$ (SFLSQ)	0.749 Fe ± .003 0.251 Mg ± .003	0.967 Fe ± .006 0.033 Ca ± .006	0.436	1.716	—	0.251	0.033
X-ray diffraction; total Fe fixed at 1.700 (RFINE)	0.743 Fe ± .003 0.257 Mg ± .003	0.957 Fe ± .003 0.043 Ca ± .003	0.437	(1.700)	—	0.257	0.043
Gamma ray resonant absorption; at liquid nitrogen temperature	0.760 Fe^{2+} ± .002 (0.240 Mg)	0.940 Fe^{2+} ± .002 (0.020 Mg)	0.447	(1.700)	0.008[c]	(0.260)	(0.040)
Gamma ray resonant absorption; at room temperature	0.745 Fe^{2+} ± .004 (0.255 Mg)	0.955 Fe^{2+} ± .004 (0.005 Mg)	0.438	(1.700)	0.008[c]	(0.260)	(0.040)
Microprobe analysis	—	—	—	1.700	—	0.257	0.038

[a] Mn, Ti, Al^{IV} ignored; values in parentheses are assumed.
[b] Where total $M2$ occupancy = 0.96, the remainder is assumed to be 0.04 Ca.
[c] Area ratio Fe^{3+}-doublet/total resonant absorption.

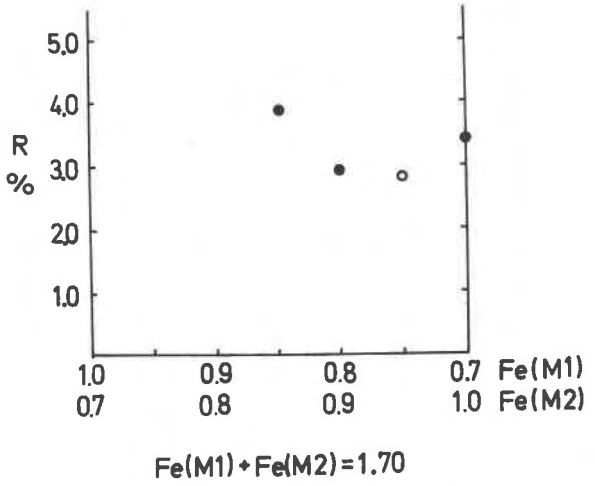

FIG. 1. Plot of R-value vs. Fe occupancy factors. The open circle denotes the final R for the accepted least-squares solution

ing site occupancy refinement (Finger, 1969), we felt that further occupancy variation subject to the condition that Fe total to 1.7 atoms would provide a check of the SFLSQ results. Two cycles of least-squares using RFINE yielded essentially the same site populations, listed in row 3 of Table 2. Atomic positional parameters changed only in the fourth decimal place.

The apparent atomic thermal ellipsoids obtained from RFINE anisotropic temperature factors show the same degree of anisotropy and the same orientations (within the standard error) as those from SFLSQ. However, the magnitudes of vibration are lower by approximately 15 to 20 percent for metal atoms, by 5 to 10 percent for Si, and by approximately 5 percent for oxygen atoms. The equivalent isotropic temperature factor of $M1$ decreased from 0.59 to 0.38, that of $M2$ from 0.82 to 0.60, and those for Si and oxygen atoms decreased by smaller amounts. The atomic scattering factors used with RFINE are those given by Cromer and Mann (1968) for ionized cations and O^{-1}, derived from Hartree-Fock wave functions neglecting relativistic effects. Above about 0.5 in $\sin\theta/\lambda$ the Hartree-Fock values are lower than those of the Thomas-Fermi-Dirac model used by SFLSQ. This difference causes the discrepancy in apparent vibration magnitudes, which combine to yield the same effective room-temperature scattering power.

Since discrepancies in vibration magnitudes represent compensation for discrepancies in high-angle scattering power, any analysis of apparent thermal motion based on absolute magnitudes of vibration is not very meaningful. Yet the relative apparent anisotropy and the orientation of the thermal ellipsoids seem insensitive to inaccuracies in at-rest scattering power, and it is these properties of the vibrational models upon which our discussion will be based.

Final R values are listed in Table 3. Atomic parameters and temperature factors are given in Table 4, bond distances and angles in Table 5, and thermal ellipsoid data in Table 6.[1]

[1] A table listing observed and calculated structure factors may be ordered as NAPS Document 01381 from National Auxiliary Publications Service of the A.S.I.S., c/o CCM Information Corporation, 909 Third Avenue, New York, N.Y. 10022; remitting in advance $2.00 for microfiche or $5.00 for photocopies, payable to CCMIC-NAPS.

TABLE 3. DISCREPANCY FACTORS, R, FOR XYZ ORTHOPYROXENE

Refinement conditions	All observations (1926)		Unrejected observations		
	Unweighted R	Weighted R	Unweighted R	Weighted R	No. of obs.
0.04 Ca in $M2$, fixed	.046	.037	.031	.023	1496
Mg omitted from $M2$	.045	.035	.035	.024	1501
Total Fe fixed at 1.700	.045	.038	.029	.023	1497

$$R_{\text{unweighted}} = \frac{\Sigma \big| |F_0| - |F_c| \big|}{\Sigma |F_0|} \qquad R_{\text{weighted}} = \left[\frac{\Sigma w(F_0 - F_c)^2}{\Sigma w F_0^2}\right]^{1/2}$$

Resonant Absorption Experiments. Our gamma-ray spectrometer consisted of a 400 channel analyzer operated in time mode in conjunction with a constant acceleration electromagnetic velocity generator. The velocity wave form was a symmetric triangle with peak velocities of ± 4 cm/sec. The velocity increment per channel was 0.04 cm/sec., and the deviation from constant acceleration never exceeded two percent. The frequency of the generator was 12.5 HZ which corresponded to 200 μsec per channel. The gamma-ray source was moved with respect to the fixed absorber with an amplitude of less than 0.1 mm, and the source-absorber distance was at least five inches; solid angle effects were tested by use of two different absorber discs with 1 and 0.5 inch diameters. They were found to be negligibly small. The full widths at half-peak height of an 0.001 inch thick metallic iron absorber were under optimum conditions 0.23 ± 0.01 (standard error) mm/sec for the two inner peaks and 0.27 ± 0.01 mm/sec for the two outer peaks (Table 7). Homogeneously distributed absorbers were prepared by mixing the powdered XYZ specimen with transoptic powder and pressing to a disc. The XYZ powder consisted of equant grains; no preferred orientation in the discs could be detected. This was concluded from Mössbauer spectra taken with the disc oriented in perpendicular as well as in a 45° position with respect to the gamma beam.

The resonant absorption spectrum of ^{57}Fe in orthopyroxene consists of two superimposed quadrupole-split doublets which can be assigned to Fe^{2+} at the $M1$ and $M2$ positions (Fig. 2). The splitting of the $M1$ doublet depends on the temperature, especially between 300 and 100°K; the splitting of the $M2$ doublet is nearly invariant in that temperature range. At room temperature, the two doublets overlap considerably, whereas at liquid nitrogen temperatures they are well separated (Fig. 2). In the present study, spectra of absorbers held at both room and at liquid nitrogen temperatures were analyzed.

Room Temperature Spectra. Care was taken to keep scattering radiation effects as small as possible. For this reason a weak source of 5 mC ^{57}Co diffused into palladium with an active area of 0.3 cm^2 was used. Four absorbers with different thicknesses were prepared (cf. Table 7). Saturation effects such as line-width broadening and deviation of the line shape from

TABLE 4. ATOM PARAMETERS[a] AND TEMPERATURE FACTORS[b] OF XYZ ORTHOPYROXENE

Atom	x	y	z	$B_{equiv.}$[c]	β_{11}	β_{22}	β_{33}	β_{12}	β_{13}	β_{23}
*M*1	0.37566 (3)	0.65424 (5)	0.87451 (9)	0.588 (9)	0.00043 (1)	0.00192 (4)	0.00506 (14)	−0.00001 (2)	−0.00010 (3)	−0.00012 (7)
*M*2	0.37795 (2)	0.48456 (4)	0.36682 (9)	0.821 (8)	0.00060 (1)	0.00288 (4)	0.00646 (13)	−0.00012 (2)	−0.00046 (3)	0.00013 (6)
Si*A*	0.27194 (4)	0.33944 (8)	0.04905 (15)	0.405 (9)	0.00022 (2)	0.00158 (7)	0.00366 (20)	−0.00008 (3)	0.00007 (5)	−0.00012 (12)
Si*B*	0.47343 (4)	0.33490 (9)	0.79113 (14)	0.423 (10)	0.00026 (2)	0.00159 (7)	0.00364 (21)	0.00008 (3)	0.00000 (6)	0.00014 (12)
O1*A*	0.18427 (10)	0.33889 (21)	0.03899 (37)	0.520 (26)	0.00022 (4)	0.00194 (18)	0.00567 (61)	0.00000 (9)	0.00010 (14)	−0.00025 (33)
O2*A*	0.31130 (11)	0.49661 (20)	0.05755 (37)	0.572 (28)	0.00047 (5)	0.00157 (18)	0.00513 (61)	−0.00016 (9)	−0.00010 (15)	−0.00015 (31)
O3*A*	0.30229 (11)	0.23575 (21)	−0.18414 (40)	0.640 (29)	0.00032 (5)	0.00301 (20)	0.00455 (66)	−0.00004 (8)	0.00004 (16)	−0.00106 (29)
O1*B*	0.56154 (10)	0.33620 (21)	0.78991 (38)	0.600 (27)	0.00024 (5)	0.00227 (19)	0.00662 (62)	0.00000 (9)	−0.00001 (15)	0.00023 (33)
O2*B*	0.43335 (11)	0.48202 (20)	0.69459 (39)	0.683 (30)	0.00053 (5)	0.00203 (19)	0.00612 (66)	0.00025 (8)	0.00041 (16)	0.00051 (30)
O3*B*	0.44735 (11)	0.20274 (20)	0.58737 (40)	0.657 (30)	0.00037 (5)	0.00259 (19)	0.00569 (69)	−0.00014 (8)	0.00017 (16)	−0.00113 (29)

[a] Atom notation is analagous to that for $P2_1/c$ clinopyroxenes in Burnham *et al* (1967); all atoms are in the general position; least-squares standard errors in parenthesis.

[b] The anisotropic temperature factor form is $\exp\{-\Sigma_i\Sigma_j\beta_{ij}h_ih_j\}$

[c] The equivalent isotropic temperature factor is computed according to $B_{equiv.}=4/3\Sigma_i\Sigma_j\beta_{ij}\mathbf{a}_i\cdot\mathbf{a}_j$, and is related in the standard way to a vibration sphere that approximates the vibration ellipsoid described by the anisotropic temperature factor tensor (Hamilton, 1959).

TABLE 5. BOND DISTANCES AND ANGLES IN XYZ ORTHOPYROXENE

M–O Distances, Å

*M*1 Octahedron		*M*2 Octahedron	
*M*1(1)–O1*A*(10)	2.076	*M*2(1)–O1*A*(10)	2.161
*M*1(1)–O1*A*(13)	2.178	*M*2(1)–O1*B*(5)	2.130
*M*1(1)–O2*A*(11)	2.086	*M*2(1)–O2*B*(1)	1.997
*M*1(1)–O1*B*(12)	2.186	*M*2(1)–O2*A*(1)	2.035
*M*1(1)–O1*B*(9)	2.106	*M*2(1)–O3*A* (7)	2.444
*M*1(1)–O2*B*(1)	2.106	*M*2(1)–O3*B*(14)	2.576
Mean	2.123	Mean	2.224

Estimated Standard Error *M*–O = 0.002 Å

O–O Distances in Cation Octahedra, Å

*M*1 Octahedron		*M*2 Octahedron	
O1*A*(10)–O1*A*(13)	3.073 Å	O1*A*(10)–O1*B*(5)	2.740 Å
O1*A*(10)–O2*A*(11)	3.098	O1*A*(10)–O2*B*(1)	2.823
O1*A*(10)–O1*B*(12)	2.900	O1*A*(10)–O2*A*(1)	2.929
O1*A*(10)–O2*B*(1)	2.823	O1*A*(10)–O3*A*(7)	3.779
O1*B*(9)–O1*A*(13)	2.900	O1*B*(5)–O2*B*(1)	3.025
O1*B*(9)–O2*A*(11)	2.898	O1*B*(5)–O2*A*(1)	2.898
O1*B*(9)–O1*B*(12)	3.048	O1*B*(5)–O3*B*(14)	3.377
O1*B*(9)–O2*B*(1)	3.162	O2*B*(1)–O3*A*(7)	3.691
O1*A*(13)–O2*A*(11)	3.095	O2*B*(1)–O3A(14)	3.602
O2*A*(11)–O2*B*(1)	2.946	O2*A*(1)–O3*A*(7)	2.503
O2*B*(1)–O1*B*(12)	3.202	O2*A*(1)–O3*B*(14)	3.088
O1*B*(12)–O1*A*(13)	2.841	O3*A*(7)–O3*B*(14)	2.941
Mean	2.999	Mean	3.116

Estimated Standard Error O–O = 0.003 Å

O–*M*–O Angles, deg.

*M*1 Octahedron		*M*2 Octahedron	
O1*A*(10)–*M*1(1)–O1*A*(13)	92.5	O1*A*(10)–*M*2(1)–O1*B*(5)	82.9
O1*A*(10)–*M*1(1)–O2*A*(11)	96.2	O1*A*(10)–*M*2(1)–O2*B*(1)	85.4
O1*A*(10)–*M*1(1)–O1*B*(12)	85.7	O1*A*(10)–*M*2(1)–O2*A*(1)	88.5
O1*A*(10)–*M*1(1)–O2*B*(1)	84.9	O1*A*(10)–*M*2(1)–O3*A*(7)	110.2
O1*A*(13)–*M*1(1)–O2*A*(11)	93.1	O1*B*(5)–*M*2(1)–O2*B*(1)	94.2
O1*A*(13)–*M*1(1)–O1*B*(12)	81.2	O1*B*(5)–*M*2(1)–O2*A*(1)	88.1
O1*A*(13)–*M*1(1)–O1*B*(9)	85.2	O1*B*(5)–*M*2(1)–O3*B*(14)	91.2
O2*A*(11)–*M*1(1)–O1*B*(9)	87.5	O2*B*(1)–*M*2(1)–O3*A*(7)	112.1
O2*A*(11)–*M*1(1)–O2*B*(1)	89.3	O2*B*(1)–*M*2(1)–O3*B*(14)	103.2
O1*B*(1)–*M*1(1)–O1*B*(9)	90.5	O2*A*(1)–*M*2(1)–O3*A*(7)	67.2
O1*B*(1)–*M*1(1)–O2*B*(1)	96.5	O2*A*(1)–*M*2(1)–O3*B*(14)	83.2
O1*B*(9)–*M*1(1)–O2*B*(1)	97.3	O3*A*(7)–*M*2(1)–O3*B*(14)	71.7
Mean	90.0	Mean	89.8
O1*A*(10)–*M*1(1)–O1*B*(9)	175.8	O1*A*(10)–*M*2(1)–O3*B*(14)	170.0
O1*A*(13)–*M*1(1)–O2*B*(1)	176.6	O1*B*(5)–*M*2(1)–O3*A*(7)	151.1
O2*A*(11)–*M*1(1)–O1*B*(12)	174.1	O2*B*(1)–*M*2(1)–O2*A*(1)	173.1
Mean	175.5	Mean	164.7

Estimated Standard Error O–*M*–O 0.08°

TABLE 5.—(*Continued*)

Si–O Distances, Å

Si*A* Tetrahedron		Si*B* Tetrahedron	
Si*A*(1)–O1*A*(1)	1.614	Si*B*(1)–O1*B*(1)	1.622
Si*A*(1)–O2*A*(1)	1.595	Si*B*(1)–O2*B*(1)	1.602
Si*A*(1)–O3*A*(1)*	1.638	Si*B*(1)–O3*B*(7)*	1.660
Si*A*(1)–O3*A*(7)*	1.651	Si*B*(1)–O3*B*(1)*	1.672
Mean	1.625	Mean	1.639

* Bridging Oxygen Atoms
Estimated Standard Error Si–O 0.002 Å

O–O Distances in Si–O Tetrahedra, Å

Si*A* Tetrahedron		Si*B* Tetrahedron	
O2*A*(1)-O3*A*(1)	2.680 Å	O2*B*(1)–O3*B*(7)	2.662 Å
O2*A*(1)–O3*A*(7)	2.503	O2*B*(1)–O3*B*(1)	2.598
O2*A*(1)–O1*A*(1)	2.740	O2*B*(1)–O1*B*(1)	2.748
O3*A*(1)–O3*A*(7)	2.632	O3*B*(7)–O3*B*(1)	2.755
O3*A*(1)–O1*A*(1)	2.637	O3*B*(7)–O1*B*(1)	2.640
O3*A*(7)–O1*A*(1)	2.698	O3*B*(1)–O1*B*(1)	2.645
Mean	2.648	Mean	2.675

Estimated Standard Error O–O 0.003 Å

O–Si–O Angles, deg.

Si*A* Tetrahedron		Si*B* Tetrahedron	
O2*A*(1)–Si*A*(1)–O3*A*(1)	112.0	O2*B*(1)–Si*B*(1)–O3*B*(7)	109.4
O2*A*(1)–Si*A*(1)–O3*A*(7)	110.9	O2*B*(1)–Si*B*(1)–O3*B*(1)	105.0
O2*A*(1)–Si*A*(1)–O1*A*(1)	117.2	O2*B*(1)–Si*B*(1)–O1*B*(1)	117.0
O3*A*(1)–Si*A*(1)–O3*A*(7)	106.3	O3*B*(7)–Si*B*(1)–O3*B*(1)	111.6
O3*A*(1)–Si*A*(1)–O1*A*(1)	108.4	O3*B*(7)–Si*B*(1)–O1*B*(1)	117.1
O3*A*(7)–Si*A*(1)–O1*A*(1)	111.4	O3*B*(1)–Si*B*(1)–O1*B*(1)	106.8
Mean	111.0	Mean	111.2

Estimated Standard Error O–Si–O 0.1°

Tetrahedral Chains

A Chain		*B* Chain	
Si*A*(1)–Si*A*(14)	3.078 Å	Si*B*(1)–Si*B*(14)	3.036 Å
O3*A*(7)–O3*A*(1)–O3*A*(14)	168.8°	O3*B*(7)–O3*B*(1)–O3*B*(14)	143.9

Estimated Standard Errors Si–Si 0.001 Å
O3–O3–O3 0.1°

Coordinate transformations indicated in parentheses above are as follows:

(1) x, y, z
(2) 1/2+x, 1/2−y, −z
(3) −x, 1/2+y, 1/2−z
(4) 1/2−x, −y, 1/2+z
(5) 1−x, 1−y, 1−z
(6) 1/2−x, 1/2+y, z
(7) x, 1/2−y, 1/2+z
(8) 1/2+x, y, 1/2−z
(9) 1−x, 1−y, 2−z
(10) 1/2−x, 1−y, 1/2+z
(11) x, y, 1+z
(12) 1−x, 1/2+y, 3/2−z
(13) 1/2−x, 1/2+y, 1+z
(14) x, 1/2−y, −1/2+z

TABLE 6. THERMAL ELLIPSOID DATA FOR *XYZ* ORTHOPYROXENE[a]

Atom	Principal axis	Rms Amplitude, Å	Angle With Respect To		
			+a	+b	+c
*M*1	*X*	0.081 (1)	56 (8)°	99 (7)°	35 (7)°
	Y	.087 (1)	40 (12)	61 (17)	115 (10)
	Z	.090 (1)	109 (15)	30 (16)	67 (9)
*M*2	*X*	0.085 (1)	52 (2)	86 (2)	38 (2)
	Y	.105 (1)	58 (3)	45 (4)	118 (3)
	Z	.114 (1)	126 (3)	45 (4)	67 (3)
Si*A*	*X*	.060 (2)	164 (6)	101 (5)	79 (10)
	Y	.071 (2)	98 (10)	105 (9)	164 (9)
	Z	.082 (2)	76 (5)	161 (8)	78 (9)
Si*B*	*X*	.065 (2)	18 (13)	106 (7)	82 (19)
	Y	.071 (2)	79 (19)	82 (10)	167 (14)
	Z	.082 (2)	75 (6)	18 (7)	80 (9)
O1*A*	*X*	.061 (6)	173 (10)	89 (10)	83 (10)
	Y	.086 (5)	96 (11)	133 (31)	137 (31)
	Z	.093 (5)	86 (9)	137 (31)	47 (31)
O2*A*	*X*	.074 (6)	61 (12)	36 (16)	71 (23)
	Y	.085 (5)	89 (25)	69 (24)	159 (24)
	Z	.094 (5)	151 (11)	63 (15)	81 (25)
O3*A*	*X*	.073 (6)	121 (209)*	75 (47)	35 (170)*
	Y	.075 (6)	149 (208)*	102 (58)	118 (193)*
	Z	.116 (4)	87 (5)	160 (5)	70 (5)
O1*B*	*X*	.065 (6)	1 (8)	90 (9)	90 (8)
	Y	.094 (5)	90 (9)	50 (33)	140 (33)
	Z	.099 (5)	91 (8)	40 (33)	50 (33)
O2*B*	*X*	.080 (6)	138 (9)	56 (40)	68 (43)
	Y	.085 (5)	85 (38)	50 (38)	140 (32)
	Z	.111 (4)	48 (7)	58 (8)	58 (8)
O3*B*	*X*	.078 (6)	155 (122)*	89 (78)	65 (117)*
	Y	.079 (6)	111 (137)*	124 (8)	138 (90)*
	Z	.113 (4)	77 (6)	146 (6)	59 (6)

[a] Standard errors in parentheses; errors marked with asterisks indicate that the positions of *X* and *Y* axes in the plane normal to the *Z* principal axis are essentially indeterminant. This is expected when the cross section of the thermal ellipsoid normal to *Z* is circular or nearly so.

TABLE 7. FITTED LINE WIDTHS OF THE HYPERFINE SPECTRUM OF ^{57}Fe IN ORTHOPYROXENE *XYZ*[a] AT 77°K

mg natural Fe per cm²[b]	Number of spectra[c]	Widths (FWHH)[d] (mm/sec)					Widths constrained to be equal[e] (mm/sec)
		A_2	A_1	B_1	B_2	Average	
XYZ orthopyroxene							
3.4	4	0.287 (0.028)	0.250 (0.016)	0.258 (0.012)	0.267 (0.016)	0.266 (0.010)	
4.8	4	0.269 (0.008)	0.271 (0.008)	0.279 (0.006)	0.270 (0.010)	0.272 (0.004)	0.273 (0.006)
6.8	4	0.278 (0.008)	0.285 (0.008)	0.282 (0.008)	0.275 (0.012)	0.279 (0.004)	0.280 (0.008)
10.2	2	0.287	0.280	0.285	0.278	0.282 (0.012)	
Metallic iron (0.001 inch foil), four inner peaks							
20.0	8	0.265 (0.002)	0.236 (0.009)	0.234 (0.010)	0.265 (0.004)	—	—

[a] Standard errors in parentheses.
[b] The samples were mixed with sieved transoptic powder of equal grain size until they were optically completely homogeneous. No pyroxene clustering (clouds in the disc) could be visually detected.
[c] "Left" and "right" counted separately.
[d] 13-variable fits; A and B are low- and high-velocity peaks and 1 and 2 refer to $M1$ and $M2$, respectively.
[e] 10-variable fits.

Lorentzian shape were found to be nearly negligible. Absorber thicknesses corresponding to 3–5 mg natural iron per cm² as commonly used for orthopyroxene spectra (Evans, *et al.*, 1967, Virgo and Hafner, 1969) can be considered as very thin. No thickness corrections need be applied when only area ratios of doublets with similar intensities are of concern, as in the case of the XYZ orthopyroxene (*cf.* Table 7, footnote a). The ratio of maximum resonant absorption (low-velocity peak of the $M2$ doublet) to the off-resonance count rate was 11 percent for the XYZ absorber with 4.8 mg natural iron per cm².

Liquid Nitrogen Spectra. The absorbers were held at atmospheric pressure in a cryostat isolated with styrofoam, as described by Virgo and Hafner (1969). The source (approximately 10 mC ^{57}Co diffused into palladium) was held at room temperature. The contribution of scattering effects to the background was approximately 10 percent higher than in room-temperature spectra. In order to exclude large temperature gradients over the absorber area the absorber was mounted between two beryllium discs and well shielded in a vacuum cryostat. The temperature was measured at the center as well as at the rim of the absorber area. It varied less than a degree. No difference compared to the spectra of the styrofoam cryostat could be detected.

Room and liquid nitrogen temperature spectra were decomposed into four Lorentzian curves by least-squares fitting of raw analyzer data using 13 variables: one for the off-resonance count rate ("background") and three for each Lorentzian. No corrections were applied for such factors as slightly variable acceleration of the moving source or solid angle effect. A very small peak due to Fe^{3+} could be observed in the XYZ spectra at approximately 0.7 mm/sec (77°K) but this peak was generally ignored in most of the fits. The 13-

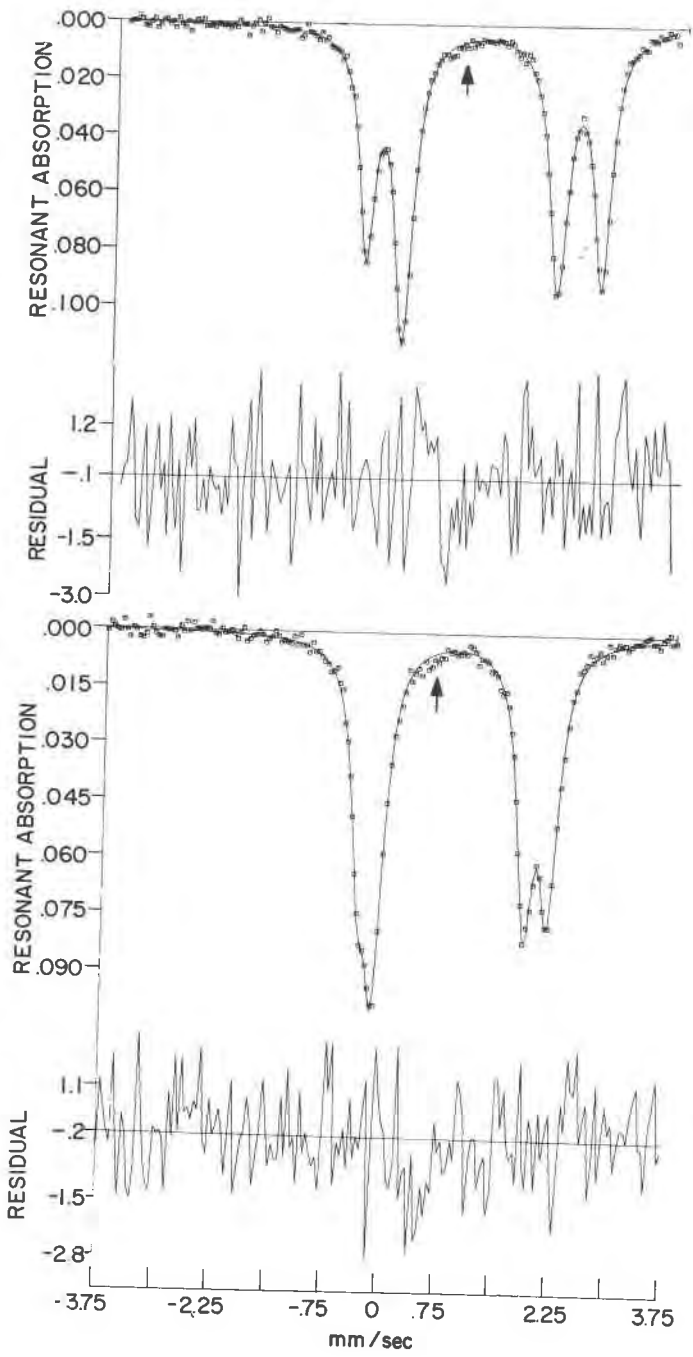
RESONANT ABSORPTION
.000
.020
.040
.060
.080
.100
RESIDUAL
1.2
-.1
-1.5
-3.0
RESONANT ABSORPTION
.000
.015
.030
.045
.060
.075
.090
RESIDUAL
1.1
-.2
-1.5
-2.8
-3.75
-2.25
-.75
0
.75
2.25
3.75
mm/sec

variable fits were statistically nearly acceptable. To retain some control over the characteristics of the velocity generator, the "left" and "right" sides (200 channels each) of the mirror-symmetric spectrum were separately fitted. The average of the squared deviations Δ^1 or contribution per channel to the χ^2 of the spectrum varied between 1.1 and 1.3 units (the count rate per channel at off-resonance velocities was approximately 0.5×10^6). This χ^2 is not higher than that obtained from the four inner lines of a 0.001 inch thick metallic iron absorber.

Line widths of the fitted room temperature spectra are shown in Table 7. The widths of all four peaks are the same within experimental error. The widths of the fitted Lorentzians have standard errors larger than those of the heights; this result is more pronounced with the liquid nitrogen spectra. Nevertheless no correlation was observed between apparent width and height. When the spectra were fitted to four Lorentzians constrained to have equal widths, χ^2 increased by an average of 0.005−0.020 units per channel (one to four units per spectrum). One may assume, therefore, that the areas of the peaks are proportional to their heights.

At temperatures below 77°K considerable complexities occur in the XYZ spectrum due to paramagnetic relaxation phenomena of the ferrous ions (Shenoy, *et al.*, 1960). At liquid nitrogen temperature, however, no significant differential broadening of the lines or deviations from Lorentzian shape could be detected.

If the absorber is very thin the fractions (distribution numbers) t_{M1} and t_{M2} of Fe^{2+} at the $M1$ and $M2$ sites will be related to the areas A_{M1} and A_{M2} of the two ^{57}Fe hyperfine doublets according to the relation.

$$t_{M1}/t_{M2} = (A_{M1}/f_{M1})/(A_{M2}/f_{M2}) \tag{1}$$

In equation (1) f_{M1} and f_{M2} are the recoil-free fractions, *i.e.* those fractions of the 14.3 keV gamma rays which are resonantly absorbed by ^{57}Fe at the sites. Since in each case the areas of the doublets were found to be proportionally related to the absorber weight within the experimental error, our absorbers may be considered as thin (*cf.* Table 7). The recoil-free fractions, f_{M1} and f_{M2} at the $M1$ and $M2$ sites are theoretically not identical. Although they are variables of the solid solution they are expected to be very nearly the same, in particular for sites with the same type of nearest-neighbor atoms and the same coordination number. The recoil-free fractions of ^{57}Fe at the tetrahedrally and octahedrally coordinated sites in stoichiometric magnetite are the same within an experimental error of less than two percent (Hafner, *et al.*, 1970). Similarly, the recoil-free fractions of ^{57}Fe at $M1$ and $M2$ in orthoferrosilite were also found to be the same within a few percent (Virgo and Hafner, 1968). In the latter case, a precise determination of the difference between

[1] $\Delta^2=(x_i-X_i)^2/x_i$, where x_i is the observed count rate and X_i the calculated rate.

←

FIG. 2. Gamma-ray resonant absorption spectrum of ^{57}Fe in XYZ orthopyroxene (4.8 mg iron per cm^2). Lower spectrum: absorber at room temperature. Upper spectrum: absorber at 77°K. The doublet with the larger splitting (3.1 mm./sec. at 77°K) is due to Fe^{2+} at $M1$; the doublet with the smaller splitting (2.0 mm./sec. at 77°K) is due to Fe^{2+} at $M2$. Arrows indicate a very small peak due to Fe^{3+}. Solid lines are least-squares fits (13 variables) neglecting Fe^{3+}. Normalized deviations $[(x_i-X_i)x_i^{\frac{1}{2}}$, cf. text] of the fits from the data are plotted below each spectrum.

TABLE 8. Fe^{2+} DISTRIBUTION OVER $M1$ AND $M2$ IN XYZ ORTHOPYROXENE DETERMINED FROM MÖSSBAUER SPECTRA[a]

Temperature of absorber	Number of spectra[b]	Fe^{2+} distribution numbers			
		from peak heights		from peak areas	
		t_{M1}	t_{M2}	t_{M1}	t_{M2}
Room temperature 13-variable fits	24	0.438 (0.004)	0.562 (0.004)	0.438 (0.005)	0.562 (0.005)
Room temperature 10-variable fits	8	0.438 (0.003)	0.562 (0.003)	0.438 (0.003)	0.562 (0.003)
77°K	14	0.447 (0.002)	0.553 (0.002)	0.426[c] (0.004)	0.574[c] (0.004)

[a] Standard errors in parentheses.

[b] "Left" and "right" counted separately.

[c] The discrepancy between the peak "area" and peak height ratios is due to a small increase of the *apparent* widths fitted to the $M2$ peaks compared to the widths of the $M1$ peaks. The apparent increase may be due to small deviations in the peak trails from Lorentzian shape at 77°K.

f_{M1} and f_{M2} is an involved problem in view of the great difficulty in synthesizing a pure, homogeneous, exactly stoichiometric phase. However, the slight areal increase of the $M1$ doublet with respect to the $M2$ doublet in XYZ (Table 8) at low temperature suggests that f_{M1} and f_{M2} are *not* identical, though the difference will certainly be small, particularly at low temperatures. Assuming then, that

$$f_{M1} = f_{M2}$$

the fractions t_{M1} and t_{M2} referred to one Fe^{2+} are obtained from the relations

$$t_{M1} = A_{M1}/(A_{M1} + A_{M2}) = (I_{A1} + I_{B1})/(I_{A1} + I_{B1} + I_{A2} + I_{B2}) \quad (2)$$

$$t_{M2} = A_{M2}/(A_{M1} + A_{M2}) = (I_{A2} + I_{B2})/(I_{A1} + I_{B1} + I_{A2} + I_{B2}). \quad (3)$$

Here I is the peak height and the subscripts A1, B1, A2, B2 refer to the low and high velocity peaks of the $M1$ and $M2$ doublets, respectively. The very small amount of ferric iron ($Fe^{3+}/Fe_{tot} \approx 0.08$) can be safely neglected. t_{M1} and t_{M2} determined by use of equations (2, 3) are shown in Table 8.

The Fe^{2+} site occupancies were obtained by multiplication of t by the analytically determined total amount of iron per six oxygen atoms (analysis 3 of Table 1). It should be noted that this occupancy determination does not depend on any assumption regarding the Mg, Ca, Mn, Ti, and Al distribution over the $M1$ and $M2$ sites. However, it requires that the total amount of iron in the crystal structure of the XYZ orthopyroxene be accurately known, i.e. it is based on the assumption that none of the M-cations are partly concentrated in exsolved cryptolamellae. No attempt has been made to determine the Fe^{2+} site occupancy from absolute intensity measurements of the doublets.

The nuclear quadrupole splittings and isomer shifts at room temperature and 77°K are listed in Table 9.

TABLE 9. NUCLEAR QUADRUPOLE SPLITTINGS AND ISOMER SHIFTS OF ^{57}FE IN *XYZ* ORTHOPYROXENE

Absorber temperature	Δ[a,b] (mm/sec)		Isomer shift[a,c] (mm/sec)	
	*M*1	*M*2	*M*1	*M*2
Room temp.	2.48	1.96	1.17	1.13
77°K	3.11	2.04	1.29	1.26

[a] Standard errors: ±0.01 mm/sec.
[b] Δ = peak separation (quadrupole splitting).
[c] Referred to metallic iron at room temperature.

DISCUSSION

Cation Distribution. One of the interesting results is the almost complete ordering of Mg^{2+} in the *M*1 site. There is little doubt that any Ca^{2+} will be restricted to *M*2, and when the analyzed amount in this sample is accounted for, both X-ray diffraction and resonant absorption data indicate that the remaining *M*2 sites are filled almost exclusively with Fe^{2+}. In an orthopyroxene of almost identical composition from a hornfels in Manchuria, Bancroft, *et al.* (1967, specimen K23) determined by room temperature Mössbauer spectroscopy that the *M*1 site contains 0.83 Fe^{2+}, while 0.89 Fe^{2+} are assigned to *M*2 (on the basis of an assumed ratio of f_{M1}/f_{M2} equal to 0.9). That orthopyroxene has the same Ca^{2+} content as ours (~0.04 Ca per 6 oxygen atoms), thus it appears to have approximately 0.07 Mg in *M*2. If f_{M1}/f_{M2} is assumed to be one, the values become 0.88 Fe^{2+} in *M*1 and 0.84 Fe^{2+} plus 0.12 Mg in *M*2. Virgo and Hafner (1970, Table 2) obtained for the same sample the distribution number $k = 0.472$ at 77°K assuming f_{M1}/f_{M2} equal to one. This leads to an approximate value of 0.05 Mg in *M*2. According to Virgo and Hafner (1969) the natural Mg, Fe distribution over M_1 and *M*2 is primarily dependent on the cooling history in the temperature range from approximately 700 to 480°C. But for samples as rich in iron as XYZ and K23 the effect of temperature and pressure on the Mg, Fe distribution will undoubtedly be very small (Virgo and Hafner, 1969, Table 2). Unfortunately the cooling history of neither sample is available in the literature, hence it is impossible to judge whether the difference in cation distribution between the two samples is due to the petrologic setting.

The methods of determining cation distribution from X-ray diffraction data have now advanced to the stage where total chemistry can be invoked as a boundary condition in the least-squares refinement (Finger, 1969). In general, restraint of total chemistry, when known by an independent chemical analysis, is an appropriate procedure, and will tend

to reduce correlations between occupancy factors and other structure parameters. We feel, however, that when the composition is sufficiently simple, as it is in this case, possible diffraction effects of minor constituents can be ignored and one can profitably operate without chemical constraints. In essence we have made an independent check on total Fe content, since similarly scattering transition elements (Mn, Cr, Co, Ni) are either very minor or absent constituents. Table 2 indicates that agreement with the microprobe analysis is quite good; such agreement reinforces our conclusion that position, vibration, and occupancy parameters did not interact significantly in the final cycles of this least-squares problem. When the chemistry is more complex there indeed remains no way to determine occupancies of more than two atomic species on a site by X-ray means without using independent information to reduce the number of variable species.

We consider the agreement between X-ray diffraction and resonant absorption results to be good. Except for the liquid-nitrogen temperature resonant absorption results, the disagreement among the determinations of cation distribution is equal to or less than the stated standard errors, namely ± 0.003 to ± 0.006 for the X-ray experiments, and ± 0.002 to ± 0.004 for the resonant absorption results. The discrepancy between liquid-nitrogen temperature results and the others is on the order of 4σ.

It should be emphasized that the stated errors represent experimental precision only, and both experiments have neglected some identifiable systematic errors. Least-squares treatment of X-ray data ignored minor Ti, Al, and Mn reported in the chemical analysis (although Al and Mn scatter similarly to Mg and Fe respectively), and included no secondary extinction correction factor. Choice of ionization state will affect scattering factor values, but only at low scattering angles where few X-ray data were obtained. The fact that the total Fe, Ca, and (Mg+Al) contents determined by X-ray procedures agree with the microprobe data (Table 2) allows us to conclude that either the selected ionization states were nearly correct, or the selection does not significantly influence X-ray determination of metal occupancies.

Resonant absorption results also ignore the possible effects of minor elements at the $M1$ and $M2$ sites. Errors in the assumption that the recoil-free fraction of ^{57}Fe resonant absorption is the same at both sites will effect the occupancy factors. Indeed slight changes in the recoil-free fractions with temperature probably explain the discrepancy between room and liquid-nitrogen temperature resonant absorption results.

$M1$ and $M2$ Coordination Polyhedra. The coordination polyhedron around the $M2$ atom is more distorted from a regular octahedron than that around $M1$. The $M2$ octahedron has two long M-O distances, 2.444 Å

and 2.576 Å, to oxygens that are bonded to two silicons (O3A and O3B), whereas the other four $M2$-O distances are between 1.997 Å and 2.161 Å. In contrast, the mean M-O bond distance for the $M1$ octahedron is 2.123 Å and the maximum deviation from this value is 0.06 Å. The mean value of the O-M-O angle for antipodal oxygen atoms has, in the $M1$ octahedron, a deviation of 5° from the ideal value of 180°. This angular deviation in the $M2$ octahedron is 15°.

The mean bond distances, M-O, of both $M1$ and $M2$ polyhedra increase with the site occupancy ratio Fe/(Fe+Mg)(Fig. 3). Morimoto and Koto (1969) have indicated a linear variation of mean $M1$-O distance with occupancy, but our new data clearly show this not to be the case, even when one considers standard errors in both distance and occupancy determinations. Departure from the line joining orthoenstatite and orthoferrosilite values appears greatest for low iron occupancy, yet a new refinement of Mg-rich hypersthene (Takeda, personal communication, 1970) with about 10 percent Fe in $M1$ shows a mean $M1$-O distance lying below the linear curve. We believe the assumption of linear variation of $M1$-O with Fe/(Fe+Mg) ratio in orthopyroxene is incorrect on the basis of data now available, and that mean $M1$-O values do not provide a reliable confirmation of occupancy values.

The nature of mean $M2$-O distance variations with composition is essentially unknown at this time. Because of extreme distortion of the $M2$ polyhedron and the presence of small but varying amounts of Ca in most hypersthenes, use of mean $M2$-O distance as anything more than a very crude indicator of occupancy is unwarranted.

The observed trends in the nuclear quadrupole splittings of the $M1$ and $M2$ hyperfine doublets are consistent with the distortions of the $M1$ and $M2$ octahedra in orthopyroxenes. The smaller splitting generally reflects the higher distortion (Fig. 2). The $M2$ splitting is *larger* in XYZ than in orthoferrosilite corresponding to a somewhat less pronounced distortion, whereas the $M1$ splitting is very nearly the same in both crystal structures. Therefore, the two doublets are less separated in XYZ than in orthoferrosilite. The centers of gravity (isomer shifts) of the two doublets appear to be related to the *smallest* M-O distance of each site. The difference between the smallest $M1$-O and $M2$-O distances is less in XYZ, than in orthoferrosilite, corresponding to a smaller difference in the isomer shifts of the $M1$ and $M2$ doublets. This is indicative of a somewhat smaller covalency difference in the bonding state of Fe^{2+} at the two different sites in XYZ.

$M1$ and $M2$ Thermal Ellipsoids. The principal axes of apparent thermal vibration of the $M1$ and $M2$ atoms are almost parallel to the directions of M-O bonds. This tendency is more conspicuous in the more distorted $M2$

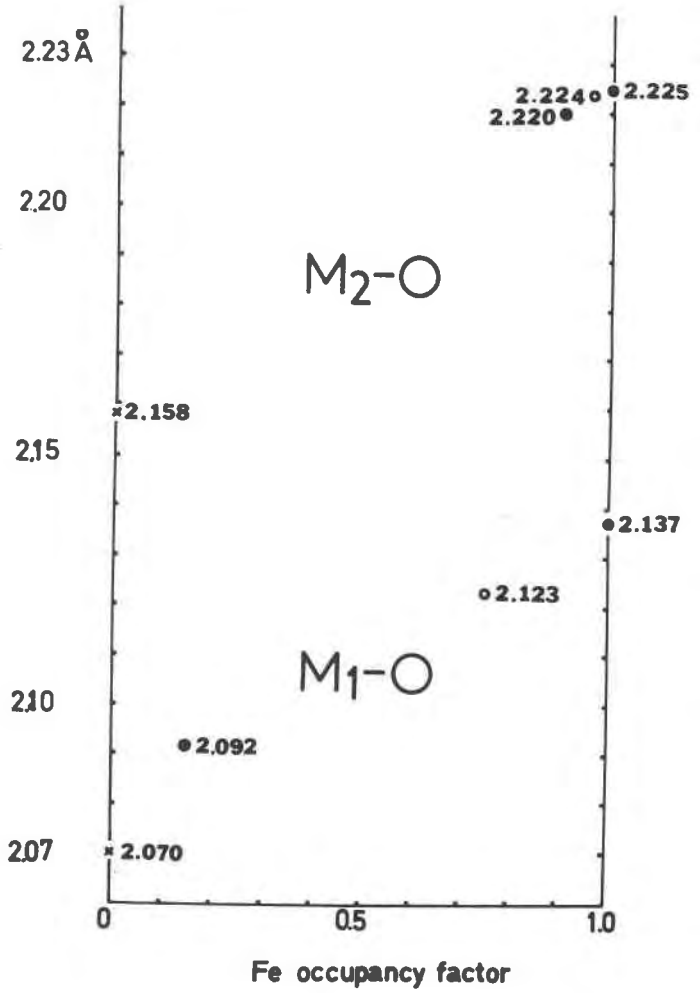

FIG. 3. Variation of mean M–O bond distance with Fe occupancy of $M1$ and $M2$ sites in orthopyroxenes. Data are for enstatite (Morimoto and Koto, 1969), hypersthene (Ghose, 1965), orthoferrosilite (Burnham, 1971), and XYZ orthopyroxene.

octahedron. The degree of anisotropy is also more marked in $M2$. The axis of maximum rms displacement corresponds to the direction between the two antipodal oxygens furthest apart in the octahedron, and the axis of minimum rms displacement to the shortest antipodal direction. These relations are shown stereographically in Figure 4.

The apparent equivalent isotropic temperature factors for $M1$ and $M2$ are 0.59 and 0.82 respectively. These values are very close to the values of

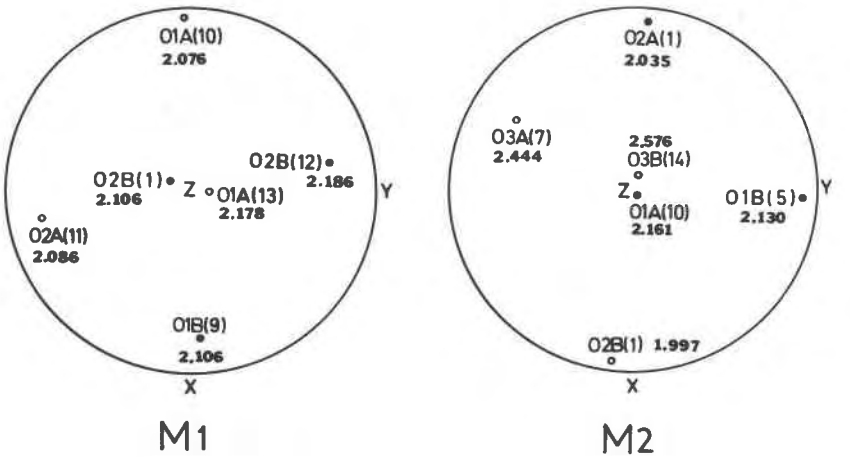

FIG. 4. Stereographic projections of oxygen atoms coordinating the $M1$ and $M2$ sites in relation to the principle axes of apparent thermal vibration ellipsoids of $M1$ and $M2$ cations. Cations are at the center of each sphere. X, Y, and Z indicate the principle axes of apparent thermal vibration with Z normal to the plane of the diagram. X is the shortest axis, Z the longest; see Table 6 for magnitudes. Solid circles are oxygen atoms in the upper hemisphere, open circles are oxygen atoms in the lower hemisphere. Figures indicate M–O distances in Å.

0.66 and 0.81 determined for the analogous Fe-containing sites in orthoferrosilite (Charles W. Burnham, in preparation). Such agreement tends to confirm the almost total lack of Mg^{2+} in $M2$. If, in fact, more Mg^{2+} were in $M2$ the true scattering power of that site would be less than that attributed to it by the model, and compensation would have been made by increasing the apparent temperature factor to a higher value.

Comparison of apparent thermal vibration data obtained by X-ray diffraction with intensity relationships observed in the hyperfine spectra yield some interesting conclusions. The recoil-free fraction, f_M, of the 14.4 keV gamma rays at equivalent iron positions, M, is equal to

$$f_M = \exp\left[-4\pi^2\bar{\mu}^2/\lambda^2\right]$$

Here, $\bar{\mu}^2$ is the mean square of the Fe^{2+} vibrational displacements in the direction defined by the gamma ray and λ is the wave length of the gamma ray (0.861 Å). Using the equivalent isotropic temperature factors ($B_{\text{equiv.}} = 8\pi^2\bar{\mu}^2$) for either XYZ or orthoferrosilite, one derives a difference in f at the two sites of somewhat more than 10 percent. Our analysis of the resonant absorption spectra can not support such a large difference. We suggest, therefore, that the differences between the apparent equivalent isotropic thermal parameters for the two sites do not

represent purely vibrational differences but reflect, in part, differences in static electronic distribution at the sites.

Both $M1$ and $M2$ hyperfine doublets are non-symmetric with respect to the intensities of the low and high velocity peaks. As a measure of this non-symmetry, we define the parameter α as

$$\alpha = (A - B)/(A + B)$$

where A and B are the areas of the low and high velocity peaks of the doublet. α is -0.04 for the $M1$ doublet and $+0.04$ for the $M2$ doublet[1]. A non-zero value of α *may be* indicative of anisotropy in the recoil-free fractions f_{M1} and f_{M2} (Karyagin-Goldanski effect). However, the insensitivity of α with temperature suggests that the recoil-free fractions cannot be highly anisotropic and thermal vibration anisotropy may not be the only explanation for a non-zero α. At any rate, there is no indication from the hyperfine spectrum of ^{57}Fe that a significant *difference* in vibrational anisotropy exists at the two sites.

The separation of temperature factors determined by X-ray diffraction into intrinsic vibrational contributions and static contributions due to non-spherically distributed electron density is a complex and essentially unsolved problem. However by comparing diffraction and resonant absorption data, we believe that the $M2$ thermal ellipsoid, and possibly the $M1$ thermal ellipsoid as well, exhibit some static effects of bonded electrons. This is consistent with the alignment of the principle axes of the cation ellipsoids parallel to M-O directions (Fig. 4).

Comparison of the X-ray determined apparent thermal ellipsoids for the two cation sites suggests that the static effects are more pronounced in $M2$; this is also consistent with the smaller observed isomer shift of ^{57}Fe at this site compared to $M1$ (Table 9). Although slight positional disorder of Ca at $M2$ could contribute to the anisotropic electron density distribution at this site, equivalence of the XYZ ellipsoid with that for $M2$ in orthoferrosilite both in magnitude and orientation argues that we are observing primarily the behavior of Fe^{2+}. We conclude that the anisotropy of the $M2$ ellipsoid and the isomer shift are both indicative of a slightly enhanced covalent participation in the Fe^{2+}-oxygen bonds at $M2$ in agreement with the suggestion made by Ghose (1965) on the basis of bond distance relationships alone.

An additional contribution to the asymmetry parameter α of the XYZ hyperfine spectra may be due to paramagnetic relaxation phenomena of ferrous iron. In fact, using the simple stochastic model of Shenoy, *et al.* (1969) it can be shown that α has the correct sign for both doublets. However, since no significant line broadening could be observed between

[1] The standard errors of α are approximately 20 percent.

77° and 300°K, relaxation effects are considered to be small in this temperature range.

Silica Tetrahedra. In the silica tetrahedron there are two different kinds of Si-O bonds: bridging bonds to O3, and non-bridging bonds to O1 and O2. As shown in Table 5, the bridging bonds are significantly longer than the non-bridging bonds in both the SiA and SiB chains. This feature is common in the silica tetrahedra of all pyroxenes, and has been discussed in detail by several authors. Clark, Appleman, and Papike (1969), and Burnham (1967) argue from an ionic point of view that the long distances are expected because of the local surplus of charge on O3 atoms; or alternatively, that local charge balance is obtained on O3 atoms only if the bonds from Si to O3 are weaker, and hence longer, than those to O1 and O2.

Morimoto and Koto (1969) suggested that Si-O bond distances change linearly according to the Fe/(Fe+Mg) ratio of orthopyroxenes. The mean distances of *bridging* bonds obtained in our study, 1.645 Å in the SiA tetrahedron and 1.666 Å in the SiB tetrahedron fall on the curves which Morimoto and Koto proposed. However, the mean distances of *non-bridging* bonds, therefore those of all Si-O bonds, do not agree with their linear relationship (Fig. 5).

The apparent thermal motion of the Si atoms is not markedly anisotropic. There is, however, a tendency for the shortest principle axis, X, to lie nearly normal to the plane containing two bridging oxygen atoms and silicon. The longest axis, Z, lies close to the bisector of the O3-Si-O3 angle (Fig. 6). It is physically quite reasonable that the largest vibration amplitude should be directed along the bisector of the two longer Si-O bonds in each tetrahedron.

Oxygen Atoms. Crystallo-chemically two kinds of oxygen atoms can be distinguished. Each O3A and O3B is bonded to two silicon atoms and therefore is called a bridging oxygen atom. Among the non-bridging oxygen atoms, O1A and O1B have much more regular coordinations than O2A and O2B. O1A and O1B are surrounded tetrahedrally by Si (Si-O, 1.62 Å) and three metal atoms (M-O, 2.08–2.19 Å), (Fig. 7a). The coordination of Si (Si-O, 1.60 Å) and two metal atoms (M-O, 2.00, 2.19 Å) around O2A and O2B is nearly planar (Fig. 7b).

Three types of thermal vibration ellipsoids, corresponding to the above mentioned geometrical features, are observed: O1A and O1B have principle axes of vibration corresponding approximately to oblate spheroids in which the shortest axes, X, are characteristic; the principle axes of O2A and O2B correspond to triaxial ellipsoids; and O3A and O3B have

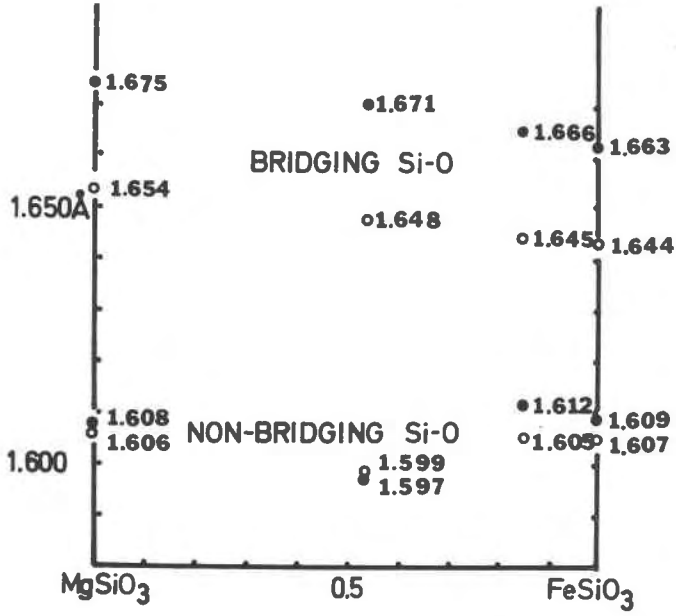

FIG. 5. Variation of mean Si-O distance with composition in orthopyroxene (Ca content ignored). Open circles are mean SiA–O distances, solid circles are mean Si*B*-O distances. Bridging Si-O is the mean of distances to two O3 atoms; non-bridging Si-O is the mean of distances to O1 and O2. References are the same as those for Fig. 3.

vibration amplitudes that may be described as prolate spheroids in which the longest axes, Z, are characteristic (Table 6). Because the point symmetry of each atom is 1, there is no symmetrical constraint on the shape or orientation of the thermal ellipsoids. The thermal vibration ellipsoids of O1A and O1B are oriented so that the shortest axis, X, is parallel to the bond to the closest-neighboring Si atom. In O3A and O3B, each of which is bonded to two Si atoms, the longest axis, Z, is roughly normal to the plane containing Si-O-Si. In the cases of O2A and O2B, the longest axis, Z, tends to be normal to the direction of the short O2-Si bonds.

It appears that the shape of thermal ellipsoids is governed by the configuration of coordinating atoms and that the shortest axis, X, is oriented parallel to the direction of the bond to the closest neighboring atom, or the longest axis, Z, is normal to that direction. Furthermore, the thermal models exhibit no positional disorder effects as might arise consequential to the random distribution of Fe^{2+} and Mg in the $M1$ site. Individual Fe^{2+}-O distances in the $M1$ polyhedra will differ from the corresponding Mg-O distances by about 0.06 Å (Fig. 3); the influence of this

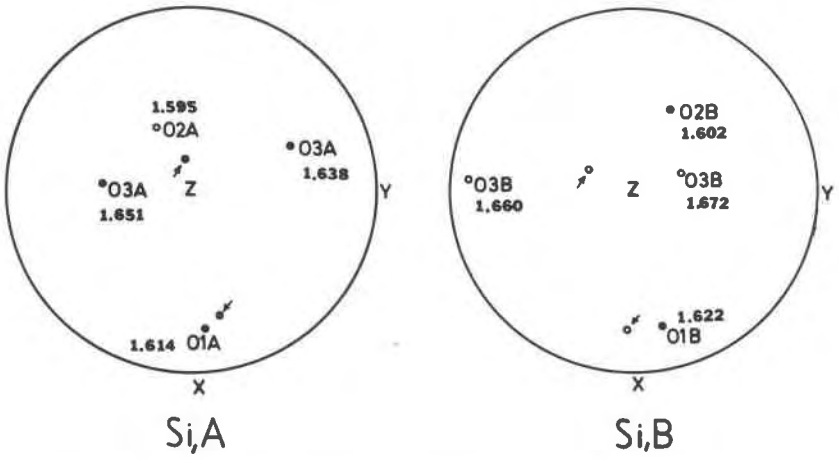

FIG. 6. Stereographic projections of oxygen atoms forming the Si*A* and Si*B* tetrahedra in relation to the principle axes of apparent thermal vibration ellipsoids of Si*A* and Si*B* cations. Convention for orientation and relative magnitudes of principle axes X, Y, and Z are the same as in Fig. 4. ↗ indicates the direction bisecting two Si-03 vectors; ↙ indicates the direction of the normal to the plane containing Si and its two coordinating O3 atoms. Figures indicate Si-O distances in Å.

difference on the apparent oxygen vibration ellipsoids is probably very small, and, in any event, is masked by the intrinsic vibrational contribution plus the competing effects of bonding to silicon and *M*2 (Fig. 7a, b).

In conjunction with our previous discussion of the *M*2 electron density distribution, it is significant to note that the *Z* principle axes of O2B, O3A, and O3B have magnitudes significantly larger than those of the longest principle axes of other oxygen atoms. Furthermore these three principle axes are aligned almost parallel to *M*2-O vectors, two of which are the extraordinarily long *M*2-O distances, and the third is along the shortest *M*2-O bond (Fig. 7). It is quite possible that these apparent vibration magnitudes do contain a contribution from static electron density anisotropy due to bonding effects, particularly in the case of O2B, whose distance along the *Z* principle axis to *M*2 is only 1.997 Å. In the case of O3A and O3B, a true vibration of the observed magnitude along the *Z* principle axis is not unlikely since the *Z* axes are essentially normal to the Si-O3-Si bridging planes. Comparison with oxygen ellipsoids in orthoferrosilite suggests that the degree of anisotropy is slightly enhanced in XYZ, probably due to the Ca in *M*2, but that the relative orientations of corresponding ellipsoids is approximately the same. Unfortunately, attempts to specifically separate vibrational from static electron density effects at this time would amount to little more than con-

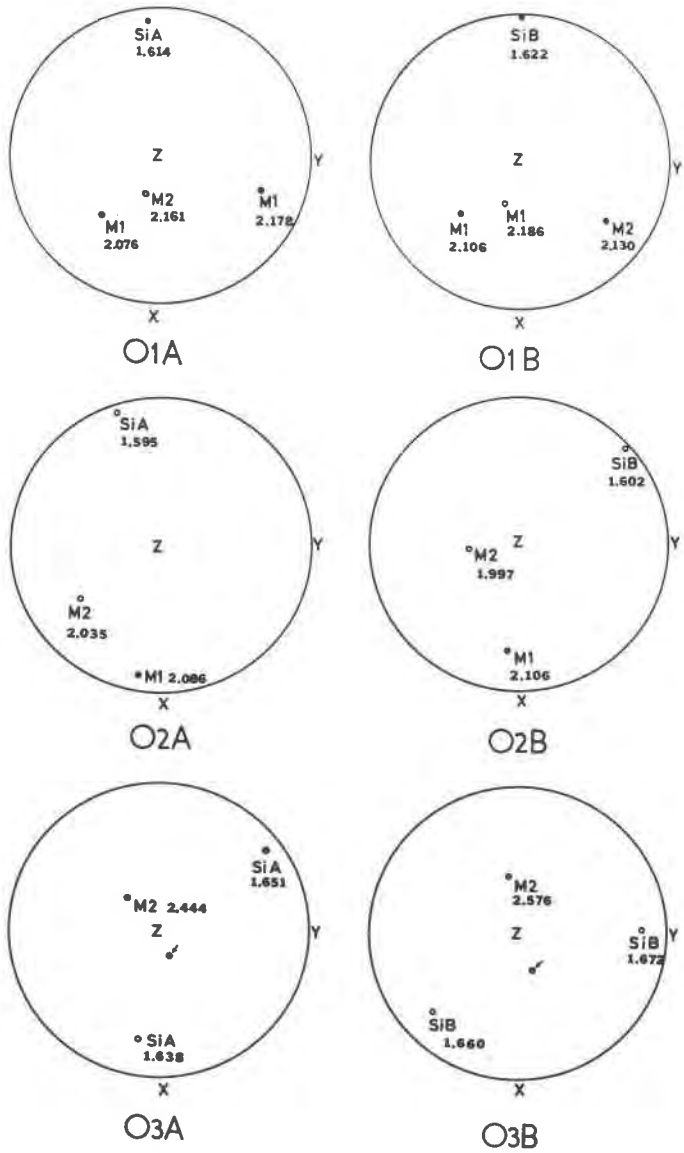

FIG. 7a, b, c. Stereographic projections of atoms coordinating oxygen atoms in relation to the principle axes of apparent thermal vibration ellipsoids of oxygen atoms; 7a plots oxygens O1, 7b plots O2, 7c plots bridging oxygens O3. Convention for orientation and relative magnitudes of principle axes X, Y and Z are the same as in Fig. 4. In Fig. 7c, ↙ indicates the direction of the normal to the plane containing the O3 oxygen and its two coordinating Si atoms. Figures indicate interatomic distances in Å.

jecture. Such analysis must await equally precise apparent vibration data obtained at low temperature.

ACKNOWLEDGMENTS

We are grateful to Professor Humberto Fernández-Morán, The University of Chicago, for his examination of XYZ orthopyroxene with the electron microscope.

The X-ray diffraction portion of this study was supported by National Science Foundation Grants GA-1130 and GA-12852 to Charles W. Burnham, and the gamma ray resonant absorption portion by National Science Foundation Grant GA-14811 to Stefan S. Hafner.

REFERENCES

BANCROFT, G. M., R. G. BURNS, AND R. A. HOWIE (1967) Determination of the cation distribution in the orthopyroxene series by Mössbauer effect. *Nature* **213,** 1221–1223.

BURNHAM, C. W. (1962) Lattice constant refinement. *Carnegie Inst. Wash. Year Book* **61,** 132–135.

——— (1966) Computation of absorption correction and the significance of end effect. *Amer. Mineral.* **51,** 159–167.

——— (1967) Ferrosilite. *Carnegie Inst. Wash. Year Book* **65,** 285–290.

BURNHAM, C. W., J. R. CLARK, J. J. PAPIKE, AND C. T. PREWITT (1967) A proposed crystallographic nomenclature for clinopyroxene structures. Z. Kristallogr. **125,** 109–119.

CLARK, J. R., D. E. APPLEMAN, AND J. J. PAPIKE (1969) Crystal-chemical characterization of clinopyroxenes based on eight new structure refinements. *Mineral. Soc. Amer., Spec. Pap.* **2,** 31–50.

CROMER, D. T., AND J. B. MANN (1968) X-ray scattering factors computed from numerical Hartree-Fock wave functions. *Acta Crystallogr.* **24,** 321–324.

EVANS, B. J., S. GHOSE, AND S. S. HAFNER (1967) Hyperfine splitting of Fe^{57} and Mg-Fe order-disorder in orthopyroxenes ($MgSiO_3$-$FeSiO_3$ solid solution). *J. Geol.* **75,** 306–322.

FERNANDEZ-MORAN, H., M. OHTSUKI, S. S. HAFNER, AND D. VIRGO (1970) High voltage electron microscopy and electron diffraction of lunar pyroxenes. *Geoch. Cosmoch. Acta Suppl. 1,* **1,** 409–417.

FINGER, L. W. (1969) Determination of cation distribution by least-squares refinement of single-crystal X-ray data. *Carnegie Inst. Wash. Year Book* **67,** 216–217.

GHOSE, S. (1965) Mg^{2+}–Fe^{2+} order in an orthopyroxene, $Mg_{0.93}Fe_{1.07}SiO_2O_6$. *Z. Kristallogr.* **122,** 81–99.

HAFNER, S. S., H. P. WEBER, AND G. KULLERUD (1970) Vacancy distribution in kenotetrahedral magnetite. *Trans. Amer. Geophys. Union* **51,** 447.

HAMILTON, W. C. (1959) On the isotropic temperature factor equivalent to a given anisotropic temperature factor. *Acta Crystallog.* **12,** 609–610.

HOWIE, R. A., AND J. V. SMITH (1966) X-ray-emission microanalysis of rock-forming minerals. V. Orthopyroxenes. *J. Geol.*, **74,** 443–462.

MORIMOTO, N., AND K. KOTO (1969) The crystal structure of orthoenstatite. *Z. Kristallogr.* **129,** 65–83.

ONKEN, H., AND K. F. FISCHER (1968) Representation and tabulation of spherical atomic scattering factors in polynominal approximation. *Z. Kristallogr.* **127,** 188–199.

PREWITT, C. T., AND C. W. BURNHAM (1966) The crystal structure of jadeite, $NaAlSi_2O_6$. *Amer. Mineral.* **51,** 956–975.

RAMBERG, H., AND G. DEVORE (1951) The distribution of Fe^{++} and Mg^{++} in coexisting olivines and pyroxenes. *J. Geol.* **59,** 193–210.

SHENOY, G. K., G. M. KALVIUS, AND S. S. HAFNER (1969) Magnetic behavior of the $FeSiO_3$-$MgSiO_3$ orthypyroxene system from NGR in ^{57}Fe. *J. App. Phys.* **40,** 1314–1316.

SMITH, J. V. (1965) X-ray-emission microanalysis of rock-forming minerals. I. Experimental techniques. *J. Geol.* **73,** 830–864.

VIRGO, D., AND S. S. HAFNER (1968) Re-evaluation of the cation distribution in orthopyroxenes by the Mössbauer effect. *Earth Planet. Sci. Lett.* **4,** 265–269.

———, ——— (1969) Fe^{2+}, Mg order-disorder in heated orthopyroxenes. *Mineral. Soc. Amer. Spec. Pap.* **2,** 67–81.

———, ——— (1970) Fe^{2+}, Mg order-disorder in natural orthopyroxenes. *Amer. Mineral.* **55,** 201–223.

Manuscript received, August 3, 1970; accepted for publication, December 23, 1970.